

Molecular coatings improve the selectivity and durability of CO₂ reduction chalcogenide photocathodes

Yungchieh Lai¹, Nicholas B. Watkins², Christopher Muzzillo³, Matthias Richter¹, Kevin Kan¹, Lan Zhou¹, Joel A. Haber¹, Andriy Zakutayev³, Jonas C. Peters^{2,*}, Theodor Agapie^{2,*}, John M. Gregoire^{1,*}

¹ Division of Engineering and Applied Science, California Institute of Technology, Pasadena, CA, USA

² Division of Chemistry and Chemical Engineering, California Institute of Technology, Pasadena, CA, USA

³ Materials Science Center, National Renewable Energy Laboratory, Golden, CO, USA

*E-mail: gregoire@caltech.edu (J.M.G.), agapie@caltech.edu (T.A.), jpeters@caltech.edu (J.C.P.)

Abstract

The quest for solar-driven conversion of carbon dioxide to chemicals and fuels hinges upon the identification of an efficient, durable, and selective photocathode. Chalcogenide p-type semiconductors exemplified by chalcopyrite Cu(In,Ga)Se₂ (CIGS) have been effectively deployed as photocathodes. However, selectivity toward CO₂ reduction and durability of the commonly used CdS adlayer remain primary challenges. Here we demonstrate that for the wide band gap CuGa₃Se₅ chalcopyrite absorber these challenges are well addressed by an organic coating generated *in situ* from an N,N'-(1,4-phenylene) bispyridinium ditriflate salt in the electrolyte. The molecular additive provides a 30-fold increase in selectivity toward CO₂R products compared to the unmodified system and lowers Cd corrosion at least 10-fold. This dual-functionality highlights the promise of hybrid solid-state-molecular photocathodes for enabling durable and efficient solar fuels systems.

Main Text

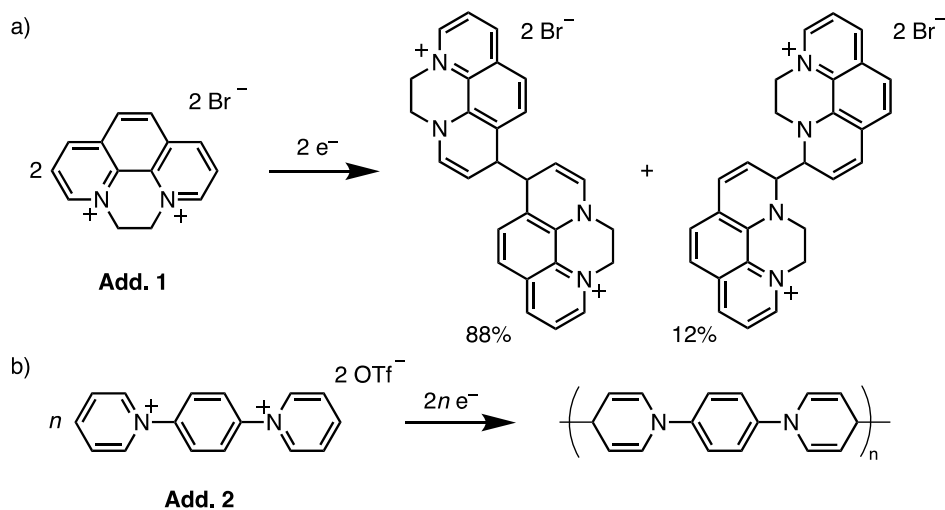
The chalcopyrite family of semiconductors, exemplified by Cu(In,Ga)Se₂ (CIGS), is one of the most important for thin films photovoltaic applications,¹ with >23% solar energy conversion efficiency demonstrated in the lab and >19% efficiency as a solar module.² While the standard CIGS absorbers have been studied as photocathodes in photoelectrochemical (PEC) water splitting applications,³⁻⁵ to increase the photovoltage a CdS layer is usually deposited to form a p-n heterojunction with the CIGS. However, due to the instability of the CdS during PEC catalysis,^{6,7} the surface is typically protected with a metal oxide (e.g. TiO₂ or ZnO) and activated with a hydrogen evolution reaction (HER) catalyst. Additionally, the 1.2-1.3 eV band gap of the most common CIGS absorber, CuIn_{0.7}Ga_{0.3}Se₂, is lower than ideal for most photoelectrochemical architectures. More recently, the wider band gap CuGaSe₂,⁸⁻¹¹ Cu(In,Ga)(S,Se)₂,^{12,13} and (Ag,Cu)GaSe₂^{14,15} chalcopyrite photocathodes have shown promise for PEC water splitting. Recent work has also expanded the use of CIGS-based photocathodes to CO₂ reduction (CO₂R).¹⁶⁻¹⁹

Among chalcopyrite absorbers, one promising CO₂R photocathode is CuGa₃Se₅, an ordered-vacancy compound derived from CuGaSe₂,²⁰ due to its wider bandgap of 1.8 eV and suitable conduction band alignment for HER and CO₂R.²¹ CuGa₃Se₅ with ZnS or CdS adlayers and platinum co-catalysts have reached photocurrent densities of 8-9 mA cm⁻² at an applied bias of 0 V vs RHE,^{22,23} and pretreated in Cd²⁺ solution with a Mg_xZn_{1-x}O capping layer demonstrates close to 1 V of photovoltage vs RHE.²⁴ In terms of stability, a bare CuGa₃Se₅ photocathode demonstrated 17 days of continuous water splitting operation,²⁵ and a WO₃-protected CuGa₃Se₅ photocathode with a Pt catalyst layer sustained solar hydrogen evolution for 6 weeks.²⁶ These reports demonstrate the photoelectrochemical stability of CuGa₃Se₅, and durable

surface modification of this material is one avenue to realize highly efficient and long-lasting fuel-forming PEC cells.

The performance of semiconductor photoelectrodes have long been modified using organic surface coatings of electrically conducting polymers to provide corrosion protection, passivate surface recombination sites, alter band edge positions by introducing dipoles at the surface, and accelerate interfacial charge separation.^{6,7,27,28} Notably, conducting polypyrrole coatings on CdS photoanodes have been shown to channel photogenerated holes to metal catalysts embedded in the polymer matrix, while preventing Cd leaching.^{6,7} Additionally, using methyl viologen as a protective conducting overlayer enhanced charge separation between Cu₂ZnSnS₄ photocathodes with inorganic buffer layers (CdS, CdSe, or ZnSe), which favorably shifts the flat band potential and improves electron transfer rates across the interface.²⁹

An open question is whether non-conductive molecular films can improve selectivity of CO₂R photocathodes while also addressing the stability issues of the CdS coating. In prior work, two N-substituted pyridinium-derived molecular additives, N,N'-ethylene-phenanthroline dibromide (**Add. 1**) and N,N'-(1,4-phenylene) bispyridinium ditriflate (**Add. 2**), have been used with Cu and/or Ag electrodes for electrochemical CO₂R. Upon *in situ* reduction and dimerization/oligomerization of the 1-electron reduced additive into a non-conductive layer on the electrode surface (Scheme 1), the metal electrocatalyst exhibits a significant decrease in activity towards hydrogen evolution in favor of CO₂ reduction.^{30–34} Mechanisms proposed to account for the change in selectivity by these and other non-conductive organic films include slow diffusion of proton carriers to the electrode, lower H₂O and increased CO₂ concentration within the films, nanostructuring of the electrode, and interactions of intermediates of CO₂ reduction on the electrode with the film.^{30–36}



Scheme 1: Electrochemical dimerization of pyridinium-based molecular additives, a) **Add. 1** and b) **Add. 2**, results in an insoluble, non-conductive film on electrode surfaces.

In this letter, we show that an organic coating derived from **Add. 1** or **Add. 2** improves both CO₂R selectivity and durability of a CdS-coated CuGa₃Se₅ photocathode. Cd corrosion and concomitant restructuring of the surface coating, as well as a H₂-rich product stream, are identified as primary shortcomings of additive-free photocathodes. Coatings formed during photoelectrochemistry in the

presence of either additive address these issues, while the conformal coating formed in the presence of **Add. 2** offers the best performance, with more than 10-fold decrease in Cd corrosion and 30-fold increase in CO:H₂.

Exploration of this new class of hybrid molecular-inorganic photocathodes was facilitated by the high throughput analytical electrochemistry (HT-ANEC, Figure 1a) screening system reported previously,³⁷ adapted in the present work to include front-side illumination for accelerated screening of CO₂R photocathodes (Figure 1b). Initial experiments conducted on a high throughput instrument (electrochemical mass spectrometry: ECMS)³⁸ revealed that CuGa₃Se₅ with a CdS coating exhibits higher photocurrent, diminished dark current, and lower FE for H₂ than the bare CuGa₃Se₅ surface (Figure S1). The observation of negligible dark current in these initial experiments down to -0.4 V vs RHE informed the choice of subsequent operating potentials between 0.2 and -0.4 V vs RHE, such that the only current measured under illumination can be assumed to be photocurrent. Continued catalyst optimization on the HT-ANEC system (Figure 1a) involved varying the illumination source, spanning from 2.1 eV (617 nm) to 3.2 eV (385 nm) at zero applied bias (Figure S2). While the 3.2 eV illumination showed higher FE toward CO, the desire to use visible illumination for solar fuels applications and the consistency in product distribution at all lower photon energies led to the choice of 2.7 eV (455 nm) illumination for further studies.

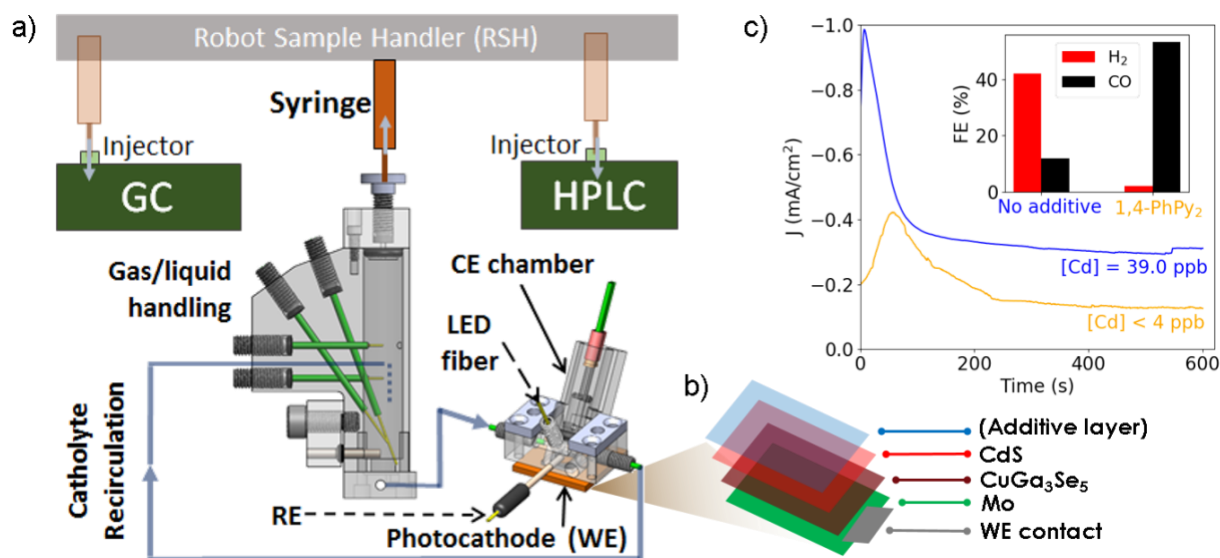


Figure 1: a) The HT-ANEC system with front-side electrode illumination includes an electrochemical reactor with fiber-coupled LED illumination, CuGa₃Se₅/CdS working electrode (WE), Ag/AgCl reference electrode (WE), and bipolar membrane-separated chamber with a Pt counter electrode (CE). Electrolyte is recirculated through the reactor and a cell with 1 atm CO₂ headspace where the reactant CO₂ as well as reaction products are equilibrated with the headspace. After electrolysis, gas and liquid aliquots are robotically sampled for product analysis. b) The multi-layer structure of the photocathode is illustrated, where the additive layer is generated *in situ* where applicable. c) Representative photoelectrocatalysis experiments at 0 V vs RHE both with and without molecular additive. Each photocurrent signal is averaged and compared to partial current densities of H₂ and CO from post-electrochemical product analysis to determine Faradaic efficiencies. The Cd concentration in electrolyte from a post-electrolysis aliquot is also shown for each experiment.

Even upon incorporation of molecular films, CO and H₂ were the only products observed in this study, making the relative partial current densities toward these products the primary results for each photoelectrolysis experiment (representative data shown in Figure 1c). Over the course of each 10 min photoelectrolysis experiment, an initial peak in photocurrent was typically observed followed by a decay to a steady-state photocurrent. We quantify the average product distribution and corrosion through characterization of the headspace and electrolyte upon conclusion of each photoelectrolysis experiment, producing results such as those indicated in the inset of Figure 1c. Inductively coupled plasma mass spectrometry (ICP-MS) was performed on post-reaction electrolytes to quantify the corrosion of Cd from the electrode into solution. X-ray fluorescence (XRF) measurements on the electrode surface were performed to confirm the changes in elemental molar loadings of the electrode (see Table S1).

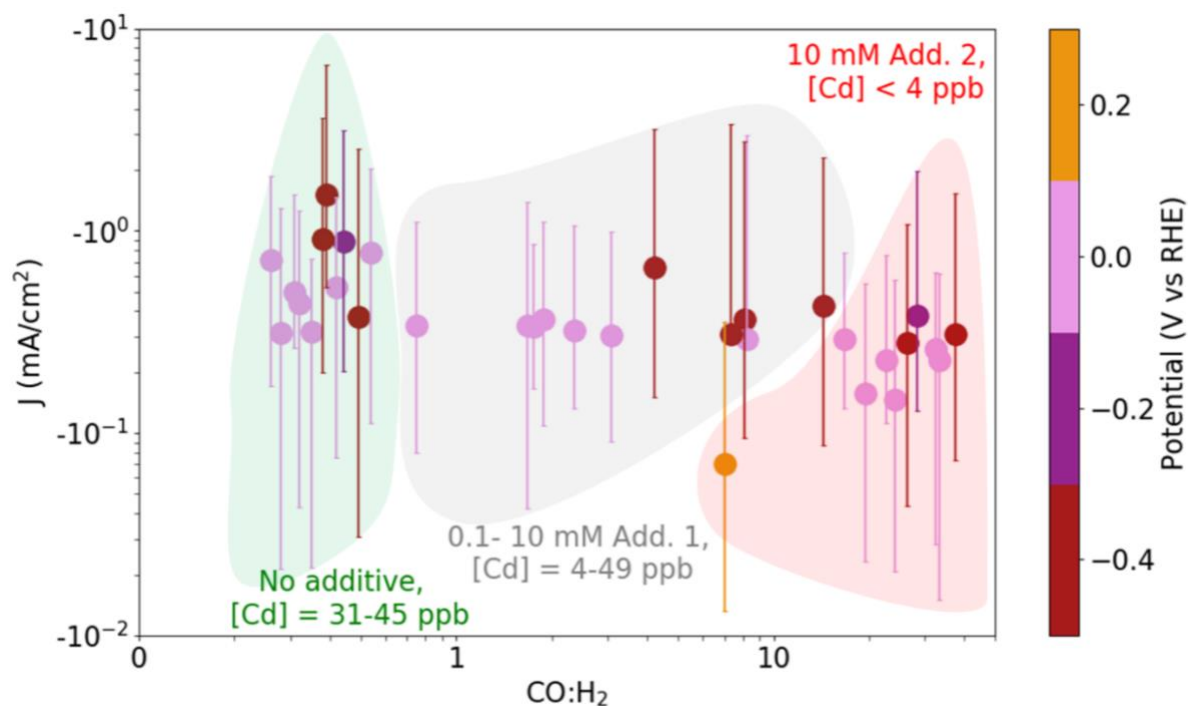


Figure 2: Summary of 32 photoelectrocatalysis experiments. For the indicated range of applied electrochemical potential, the three conditions of no additive, **Add. 1**, and **Add. 2** form clusters indicated by shaded regions, where each additive offers improved CO₂R selectivity at the expense of lowered photocurrent. The point for a given electrolysis experiment indicates the median photocurrent density with error bars extending from the minimum to maximum photocurrent density during the 10 min photoelectrolysis. The label for each cluster shows the range of Cd concentration in electrolyte observed for each condition.

The experiments performed can be delineated using the CO:H₂ product ratio and the average photocurrent density from each photoelectrolysis experiment (Figure 2). The maximum and minimum of the photocurrent density is shown as vertical error bars. As expected, changing the applied bias resulted in variation in the photocurrent and product ratio; however, these variations are relatively small compared to those observed when including a molecular additive in the electrolyte. With no additive, CO:H₂ remained below 1 for all experiments. Electrodes modified with **Add. 1** routinely produced CO:H₂ in excess of 1, and electrodes modified with **Add. 2** modified achieved CO:H₂ in excess of 30. As a result, these electrolysis experiments are cleanly clustered into three distinct groups, with each cluster labeled by the additive as well as the range of observed concentration of Cd in the electrolyte. Notably, the

presence of **Add. 2** lowers Cd levels in the electrolyte from 31-45 ppb observed in the absence of a molecular additive to below the noise level of 4 ppb. A range of concentrations of **Add. 1** were evaluated to assess any impact on product selectivity (see Table S1), and the concentration was found to be less important than the presence and choice of additive.

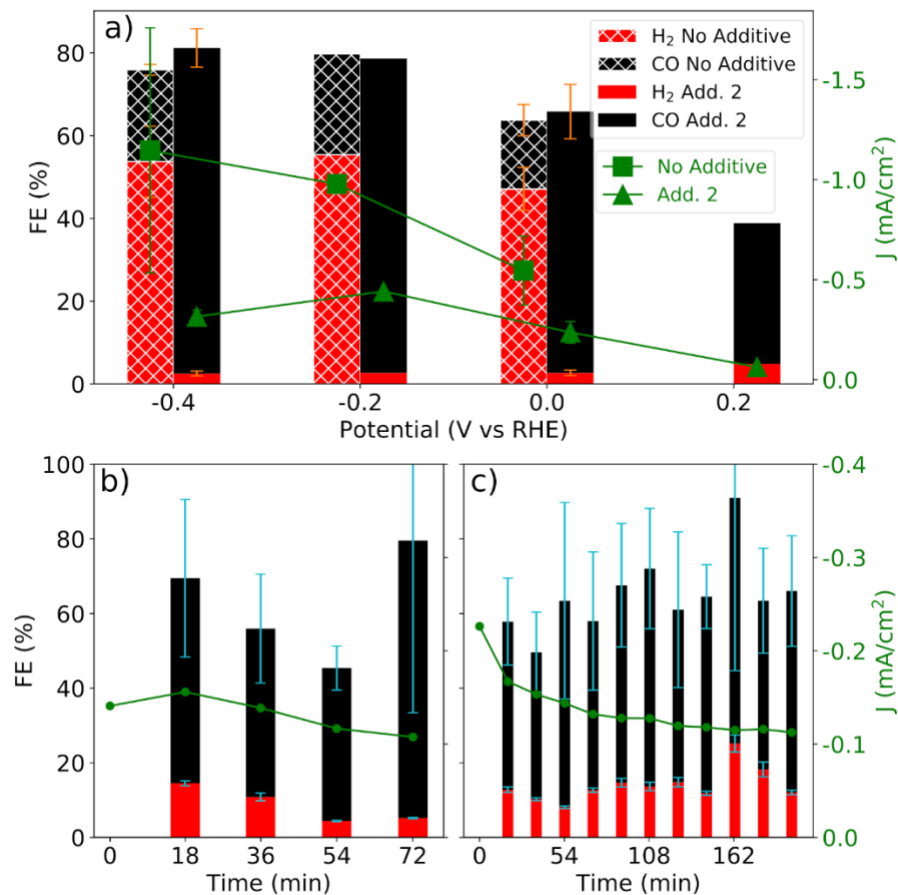


Figure 3: a) Aggregation of the experiments in Figure 2 for the no-additive and **Add. 2** conditions, showing that the presence of the additive provides high selectivity toward CO. The error bars for both FE and J at -0.4 V and 0 V vs RHE represent the standard deviation of the respective measurements over the several photoelectrocatalysis experiments shown in Figure 2. The shift of the green data points from the labeled potentials is to group them with the barplot at the same conditions (with or without **Add. 2**) and does not indicate that the potential is shifted. b) Validation of the high throughput screening results with 10 mM **Add. 2** using a traditional H-cell at 0 V vs RHE with periodic headspace measurements. c) Continued operation of the H-cell with the same electrode at the same potential but starting with additive-free electrolyte. The continued high CO selectivity and photocurrent demonstrate that the organic coating formed from the initial operation persists and remains effective at suppressing HER in favor of CO₂R to CO. The error bars in b) and c) represent the uncertainty of product quantification by the analytical instruments, and the photocurrent density (green) in these panels correspond to the right axis.

The potential-dependent selectivity and activity of CuGa₃Se₅/CdS with and without the **Add. 2** additive demonstrate how the organic film causes an increase in selectivity for CO vs. H₂ by more than 30-fold at the expense of a 2 to 4-fold reduction in photocurrent (Figure 3a). While suppression of HER appears to be a primary contributor to the decrease in photocurrent (Figure S3), the additives may also attenuate the intensity of the incident light and contribute to the observed lower photocurrent. The

partial current density for CO at 0 V vs RHE increases with **Add. 1** and even more so with **Add. 2** compared to the no-additive baseline, which may be due to retention of the Cd coating that facilitates carrier extraction from CuGa₃Se₅ as discussed further below. In dark electrolysis experiments with cathodic current densities between 0.5 and 15 mA cm⁻², the total FE of measured products can routinely be as low as 80% due to imperfect product extraction from the headspace from the HT-ANEC system.³⁷ As shown in Figure 3a, measurements at -0.2 and -0.4 V vs RHE both with and without additive result in total FE near 80%. At higher potentials, lower total FE is observed, although this may be due to the lower photocurrent densities causing lower product concentrations and thus increased systematic error in FE quantification. These results can neither confirm nor deny the presence of photoelectrochemical reactions beyond the HER and CO₂R. Possible side reactions include Cd corrosion and electrodeposition of the molecular additive, and a more quantitative evaluation of FE will be pursued in future work.

To validate the primary result of the high throughput screening, a pair of CuGa₃Se₅/CdS electrodes were tested in a traditional H-cell using 10 mM of **Add. 2** and 0 V vs RHE. One experiment involved isotopic labelling in which the cell was operated with a sealed headspace of ¹³CO₂ for 2 hours, after which photoelectrochemical operation was paused and the headspace was changed to flowing ¹³CO₂. After acquiring a background mass spectroscopy (MS) signal, photoelectrochemistry was resumed, resulting in the subsequent detection of ¹³CO in the headspace (Figure S4) and thereby confirming photoelectrochemical reduction of ¹³CO₂ to ¹³CO. The second experiment focused on stability and involved a total of 4.5 h of photoelectrolysis at 0 V vs RHE. The first 1.2 hours were conducted in the presence of 10 mM of **Add. 2**, followed by 3.3 hours with additive-free electrolyte to ascertain whether stable photocurrent and product distribution could be obtained with the already-deposited molecular coating. The photocurrent and product distribution are shown in Figure 3, which has large uncertainty for FE of CO due to the detection mechanism on this instrument. The results confirm that the high selectivity toward CO in the presence of the additive is maintained upon replacement with fresh electrolyte. While higher cathodic photocurrent is initially observed, the subsequent steady-state photocurrent is comparable to that observed with additive present in the electrolyte. Furthermore, ICP-MS characterization of the additive-free electrolyte after 3.3 hours of operation did not show any Cd in solution (Table S1). These results collectively show that **Add. 2** may be applied as a final step of electrode synthesis, resulting in an electrode that may be operated with no requirement on additive presence in the electrolyte, although the stability and possible regeneration requirements for device-scale operation remains under investigation.

Characterization of the post-catalysis electrode surfaces lends insight into the mechanism by which catalyst performance is enhanced. Tunneling electron microscopy (TEM) with energy dispersive spectroscopy (EDS) mapping was performed to compare the ca. 50 nm CdS capping layer of the as-synthesized electrode with electrodes tested by HT-ANEC at 0 V vs RHE with no additive, 0.1 mM **Add. 1**, and 10 mM **Add. 2** (Figure 4a, S7). Images and compositions of the electrode surfaces post-catalysis show that without an organic coating, the CdS layer is greatly depleted of sulfur in favor of oxygen. These observations are consistent with an electrochemical reaction that results in partial corrosion and coarsening of the adlayer, which is evident in top-down SEM and TEM images with a larger field of view that show a nanocube morphology (Figure S5a and S5c). The same phenomena are observed with **Add. 1** but to a lesser extent, which combined with our observation of variable Cd leaching concentrations (Figure 2, Table S1) suggest that this additive only partially protects the Cd-based layer. With **Add. 2**, the Cd-based coating remains compact, with a 30 nm sulfur-containing layer near the interface with the CuGa₃Se₅

absorber that is not observed in the other samples (Figure 4a, S7). This remaining CdS-like layer is key to preserving the photoactivity of CuGa_3Se_5 and other chalcogenide absorbers.²⁴

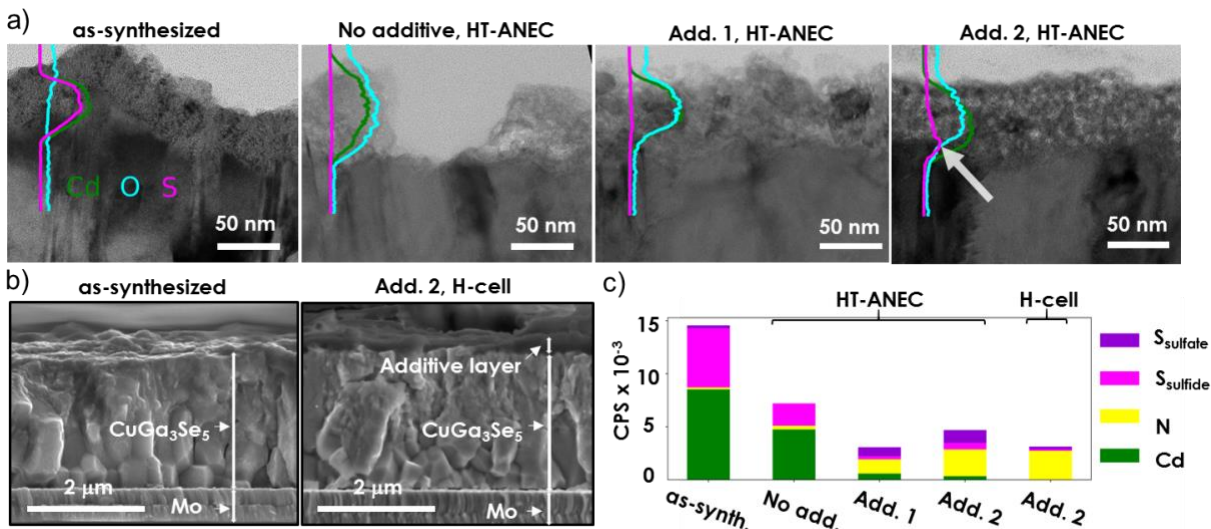


Figure 4: a) Cross section TEM measurements of the Cd-based layer and its interface to the CuGa_3Se_5 absorber layer for as-synthesized electrodes and electrodes operated at 0 V vs RHE in the HT-ANEC system with no additive and with each of the molecular additives. The overlay composition plot in each image shows the measured depth profile of Cd, S, and O concentrations from EDS line-scan imaging (see Figure S7 for additional composition data), and an arrow points to the retention of S due to the presence of **Add. 2**. Note that the lack of additives seen on TEM images is due to their low contrast to the capping agent used for preparing TEM samples. b) Cross section SEM images of an as-synthesized $\text{CuGa}_3\text{Se}_5/\text{CdS}$ electrode and the electrode with organic coating after the conclusion of the Figure 3c experiment. The coating appears conformal with approximately 200 nm thickness (see Figure S4 for more information). c) XPS characterization of the 5 conditions from a) and b) for the near-surface compositions. Other detected species can be found in Figure S6b. Note that the H-cell data in b) and c) were acquired on the electrode after both the 1.2 h operation with and the 3.3 h operation without **Add. 2**.

To understand the role of **Add. 2** in protecting the CuGa_3Se_5 photoabsorber and preserving the CdS layer, scanning electron microscopy (SEM) and X-ray photoelectron spectroscopy (XPS) measurements were performed. Analysis of the film created by **Add. 2** by cross-sectional SEM revealed that after 4.5-hours of operation, a near 200 nm conformal coating is observed with some larger features (Figure 4b and Figure S5). This result is commensurate with the reported thicknesses of electrodeposited films derived from analogous pyridinium salt precursors on copper and silver electrodes and is on average thicker than the ~30 nm film afforded by **Add. 1**.^{31,34} The **Add. 2** coating results in lower coarsening and improved retention of the CdS layer than in the other experiments, which we attribute to improved protection from its high conformality and greater thickness. XPS near-surface characterization supports the findings that the Cd and S in the as-synthesized electrode are observed to a lesser extent after operation with no additive due to corrosion and oxidation of the CdS layer (Figure 4c, S8). The Cd signal is increasingly suppressed with **Add. 1** and **Add. 2** as the molecular coatings attenuate the signals from the Cd-based layers observed in Figure 4a. While the relative impact on product selectivity and corrosion mitigation between the two additives is commensurate with the observed differences in the morphology of the generated coatings, the chemical mechanism for the absolute and relative performance enhancements will be investigated in future work.

Given the importance of CdS in passivation of surface defects for improved carrier extraction efficiency,²⁴ the ability of **Add. 2** to inhibit coarsening in the Cd-based layer, and thereby maintain sulfur in CdS at the CuGa₃Se₅ absorber interface, is an important observation. Furthermore, due to the lack of Cu, Ga, or Se leaching and the persistence of a compact Cd-based layer in the presence of either additive, we believe these results will generalize to light absorbers beyond CuGa₃Se₅. Given that CdS is an effective contact material for CIGS chalcopyrite and the multitude of other absorber chemistries,^{39,40} these additives, especially **Add. 2**, may more generally improve the stability of the Cd-based coating while substantially suppressing HER in favor of CO₂R. Differences in photovoltage provided by different absorber layers will likely alter the applied bias required to obtain the equivalent (unquantified) surface potential of the electrodes in the present work. The observation of CO₂R with high selectivity at a bias of 0.2 V vs RHE demonstrates that the turn-on potential for CO₂R photoelectrocatalysis is even higher, making these photocathodes competitive with state-of-the-art photocathodes, such as the Pt-TiO₂/GaN/n⁺-p-Si photocathodes with turn-on potentials near 0.47 V vs RHE⁴¹, and nanoporous Au thin films on Si photoelectrodes with turn-on potentials >0.2 V vs RHE.⁴² To close, molecular additives such as those described herein are attractive for the continued improvement of turn-on potential, durability, and CO₂R selectivity, which are all critical to realize photoelectrochemical generation of solar fuels.

Supporting Information

Methodologies for using the high throughput experimentation systems used herein. Molecular additive synthesis and characterization. Further description of durability testing. Combinatorial experiments for selecting electrode, illumination, and potential range; additional SEM, TEM, and XPS characterization of electrodes; table of all electrolysis and corrosion results.

Acknowledgment

This material is based on work performed by the Liquid Sunlight Alliance, which is supported by the U.S. Department of Energy, Office of Science, Office of Basic Energy Sciences, Fuels from Sunlight Hub under Award Number DE-SC0021266. National Renewable Energy Laboratory is operated by Alliance for Sustainable Energy, LLC, for the U.S. Department of Energy (DOE) under Contract No. DE-AC36-08GO28308. The Resnick Sustainability Institute at Caltech is also acknowledged for its support of enabling infrastructure and facilities. The views expressed in this article do not necessarily represent the views of the DOE or the U.S. Government.

References

- (1) Review of progress toward 20% efficiency flexible CIGS solar cells and manufacturing issues of solar modules | IEEE Conference Publication | IEEE Xplore <https://ieeexplore.ieee.org/abstract/document/6656789> (accessed 2021 -11 -05).
- (2) Green, M.; Dunlop, E.; Hohl-Ebinger, J.; Yoshita, M.; Kopidakis, N.; Hao, X. Solar Cell Efficiency Tables (Version 57). *Progress in Photovoltaics: Research and Applications* **2021**, *29* (1), 3–15. <https://doi.org/10.1002/pip.3371>.
- (3) Yokoyama, D.; Minegishi, T.; Maeda, K.; Katayama, M.; Kubota, J.; Yamada, A.; Konagai, M.; Domen, K. Photoelectrochemical Water Splitting Using a Cu (In, Ga) Se₂ Thin Film. *Electrochemistry Communications* **2010**, *12* (6), 851–853.
- (4) Mali, M. G.; Yoon, H.; Joshi, B. N.; Park, H.; Al-Deyab, S. S.; Lim, D. C.; Ahn, S.; Nervi, C.; Yoon, S. S. Enhanced Photoelectrochemical Solar Water Splitting Using a Platinum-Decorated CIGS/CdS/ZnO Photocathode. *ACS applied materials & interfaces* **2015**, *7* (38), 21619–21625.

- (5) Hadke, S.; Huang, M.; Chen, C.; Tay, Y. F.; Chen, S.; Tang, J.; Wong, L. Emerging Chalcogenide Thin Films for Solar Energy Harvesting Devices. *Chem. Rev.* **2021**, <https://doi.org/10.1021/acs.chemrev.1c00301>.
- (6) Frank, A. J.; Honda, K. Oxygen and Hydrogen Generation from Water on Polymer-Protected CdS Photoanodes. *Journal of Electroanalytical Chemistry and Interfacial Electrochemistry* **1983**, *150* (1), 673–678. [https://doi.org/10.1016/S0022-0728\(83\)80246-0](https://doi.org/10.1016/S0022-0728(83)80246-0).
- (7) Honda, K.; Frank, A. J. Polymer-Catalyst-Modified Cadmium Sulfide Photochemical Diodes in the Photolysis of Water. *J. Phys. Chem.* **1984**, *88* (23), 5577–5582. <https://doi.org/10.1021/j150667a024>.
- (8) Moriya, M.; Minegishi, T.; Kumagai, H.; Katayama, M.; Kubota, J.; Domen, K. Stable Hydrogen Evolution from CdS-Modified CuGaSe₂ Photoelectrode under Visible-Light Irradiation. *Journal of the American Chemical Society* **2013**, *135* (10), 3733–3735.
- (9) Gaillard, N.; Prasher, D.; Kaneshiro, J.; Mallory, S.; Chong, M. Development of Chalcogenide Thin Film Materials for Photoelectrochemical Hydrogen Production. *MRS Online Proceedings Library (OPL)* **2013**, *1558*.
- (10) Ikeda, S.; Fujita, W.; Okamoto, R.; Nose, Y.; Katsube, R.; Yoshino, K.; Harada, T. Preparation of a CuGaSe₂ Single Crystal and Its Photocathodic Properties. *RSC Adv.* **2020**, *10* (66), 40310–40315. <https://doi.org/10.1039/D0RA07904A>.
- (11) Ikeda, S.; Okamoto, R.; Ishizuka, S. Enhancement of the Photoelectrochemical Properties of a CuGaSe₂-Based Photocathode for Water Reduction Induced by Loading of a Cu-Deficient Layer at the p–n Heterointerface. *Appl. Phys. Lett.* **2021**, *119* (8), 083902. <https://doi.org/10.1063/5.0060494>.
- (12) Gaillard, N.; Prasher, D.; Chong, M.; Deangelis, A.; Horsley, K.; Ishii, H. A.; Bradley, J. P.; Varley, J.; Ogitsu, T. Wide-Bandgap Cu (In, Ga) S₂ Photocathodes Integrated on Transparent Conductive F: SnO₂ Substrates for Chalcopyrite-Based Water Splitting Tandem Devices. *ACS Applied Energy Materials* **2019**, *2* (8), 5515–5524.
- (13) DeAngelis, A. D.; Horsley, K.; Gaillard, N. Wide Band Gap CuGa (S, Se) ₂ Thin Films on Transparent Conductive Fluorinated Tin Oxide Substrates as Photocathode Candidates for Tandem Water Splitting Devices. *The Journal of Physical Chemistry C* **2018**, *122* (26), 14304–14312.
- (14) Zhang, L.; Minegishi, T.; Nakabayashi, M.; Suzuki, Y.; Seki, K.; Shibata, N.; Kubota, J.; Domen, K. Durable Hydrogen Evolution from Water Driven by Sunlight Using (Ag, Cu) GaSe₂ Photocathodes Modified with CdS and CuGa₃Se₅. *Chemical science* **2015**, *6* (2), 894–901.
- (15) Zhang, L.; Minegishi, T.; Kubota, J.; Domen, K. Hydrogen Evolution from Water Using Ag_xCu_{1-x}GaSe₂ Photocathodes under Visible Light. *Physical Chemistry Chemical Physics* **2014**, *16* (13), 6167–6174.
- (16) Pati, P. B.; Wang, R.; Boutin, E.; Diring, S.; Jobic, S.; Barreau, N.; Odobel, F.; Robert, M. Photocathode Functionalized with a Molecular Cobalt Catalyst for Selective Carbon Dioxide Reduction in Water. *Nat Commun* **2020**, *11* (1), 3499. <https://doi.org/10.1038/s41467-020-17125-4>.
- (17) Foster, B. M.; Paris, A. R.; Frick, J. J.; Blasini-Pérez, D. A.; Cava, R. J.; Bocarsly, A. B. Catalytic Mismatching of CuInSe₂ and Ni₃Al Demonstrates Selective Photoelectrochemical CO₂ Reduction to Methanol. **2020**, *3* (1), 109–113.
- (18) Hu, Z.; Gong, J.; Ye, Z.; Liu, Y.; Xiao, X.; Yu, J. C. Cu(In,Ga)Se₂ for Selective and Efficient Photoelectrochemical Conversion of CO₂ into CO. *Journal of Catalysis* **2020**, *384*, 88–95. <https://doi.org/10.1016/j.jcat.2020.02.015>.
- (19) Tran, P. D.; Wong, L. H.; Barber, J.; Loo, J. S. C. Recent Advances in Hybrid Photocatalysts for Solar Fuel Production. *Energy Environ. Sci.* **2012**, *5* (3), 5902–5918. <https://doi.org/10.1039/C2EE02849B>.

- (20) Zhang, S. B.; Wei, S.-H.; Zunger, A. Stabilization of Ternary Compounds via Ordered Arrays of Defect Pairs. *Phys. Rev. Lett.* **1997**, *78* (21), 4059–4062. <https://doi.org/10.1103/PhysRevLett.78.4059>.
- (21) Kim, J.; Minegishi, T.; Kobota, J.; Domen, K. Investigation of Cu-Deficient Copper Gallium Selenide Thin Film as a Photocathode for Photoelectrochemical Water Splitting. *Jpn. J. Appl. Phys.* **2012**, *51* (1), 015802. <https://doi.org/10.1143/JJAP.51.015802>.
- (22) Kim, J.; Minegishi, T.; Kobota, J.; Domen, K. Enhanced Photoelectrochemical Properties of CuGa_3Se_5 Thin Films for Water Splitting by the Hydrogen Mediated Co-Evaporation Method. *Energy Environ. Sci.* **2012**, *5* (4), 6368–6374. <https://doi.org/10.1039/C1EE02280F>.
- (23) Kumagai, H.; Minegishi, T.; Moriya, Y.; Kubota, J.; Domen, K. Photoelectrochemical Hydrogen Evolution from Water Using Copper Gallium Selenide Electrodes Prepared by a Particle Transfer Method. *J. Phys. Chem. C* **2014**, *118* (30), 16386–16392. <https://doi.org/10.1021/jp409921f>.
- (24) Khan, I. S.; Muzzillo, C. P.; Perkins, C. L.; Norman, A. G.; Young, J. L.; Gaillard, N.; Zakutayev, A. $\text{Mg}_x\text{Zn}_{1-x}\text{O}$ Contact to CuGa_3Se_5 Absorber for Photovoltaic and Photoelectrochemical Devices. *J. Phys. Energy* **2021**, *3* (2), 024001. <https://doi.org/10.1088/2515-7655/abd3b3>.
- (25) Muzzillo, C. P.; Klein, W. E.; Li, Z.; DeAngelis, A. D.; Horsley, K.; Zhu, K.; Gaillard, N. Low-Cost, Efficient, and Durable H_2 Production by Photoelectrochemical Water Splitting with CuGa_3Se_5 Photocathodes. *ACS Appl. Mater. Interfaces* **2018**, *10* (23), 19573–19579. <https://doi.org/10.1021/acsami.8b01447>.
- (26) Palm, D. W.; Muzzillo, C. P.; Ben-Naim, M.; Khan, I.; Gaillard, N.; Jaramillo, T. F. Tungsten Oxide-Coated Copper Gallium Selenide Sustains Long-Term Solar Hydrogen Evolution. *Sustainable Energy Fuels* **2021**, *5* (2), 384–390. <https://doi.org/10.1039/D0SE00487A>.
- (27) Hilal, H. S.; Turner, J. A. Controlling Charge-Transfer Processes at Semiconductor/Liquid Junctions. *Electrochimica Acta* **2006**, *51* (28), 6487–6497. <https://doi.org/10.1016/j.electacta.2006.04.035>.
- (28) Guijarro, N.; Prévot, M. S.; Sivula, K. Surface Modification of Semiconductor Photoelectrodes. *Phys. Chem. Chem. Phys.* **2015**, *17* (24), 15655–15674. <https://doi.org/10.1039/C5CP01992C>.
- (29) Rovelli, L.; Tilley, S. D.; Sivula, K. Optimization and Stabilization of Electrodeposited $\text{Cu}_2\text{ZnSnS}_4$ Photocathodes for Solar Water Reduction. *ACS Appl. Mater. Interfaces* **2013**, *5* (16), 8018–8024. <https://doi.org/10.1021/am402096r>.
- (30) Han, Z.; Kortlever, R.; Chen, H.-Y.; Peters, J. C.; Agapie, T. CO_2 Reduction Selective for $\text{C}_{\geq 2}$ Products on Polycrystalline Copper with N-Substituted Pyridinium Additives. *ACS Cent. Sci.* **2017**, *3* (8), 853–859. <https://doi.org/10.1021/acscentsci.7b00180>.
- (31) Thevenon, A.; Rosas-Hernández, A.; Peters, J. C.; Agapie, T. In-Situ Nanostructuring and Stabilization of Polycrystalline Copper by an Organic Salt Additive Promotes Electrocatalytic CO_2 Reduction to Ethylene. *Angew. Chem. Int. Ed.* **2019**, *58* (47), 16952–16958. <https://doi.org/10.1002/anie.201907935>.
- (32) Li, F.; Thevenon, A.; Rosas-Hernández, A.; Wang, Z.; Li, Y.; Gabardo, C. M.; Ozden, A.; Dinh, C. T.; Li, J.; Wang, Y.; Edwards, J. P.; Xu, Y.; McCallum, C.; Tao, L.; Liang, Z.-Q.; Luo, M.; Wang, X.; Li, H.; O'Brien, C. P.; Tan, C.-S.; Nam, D.-H.; Quintero-Bermudez, R.; Zhuang, T.-T.; Li, Y. C.; Han, Z.; Britt, R. D.; Sinton, D.; Agapie, T.; Peters, J. C.; Sargent, E. H. Molecular Tuning of CO_2 -to-Ethylene Conversion. *Nature* **2020**, *577* (7791), 509–513. <https://doi.org/10.1038/s41586-019-1782-2>.
- (33) Ozden, A.; Li, F.; García de Arquer, F. P.; Rosas-Hernández, A.; Thevenon, A.; Wang, Y.; Hung, S.-F.; Wang, X.; Chen, B.; Li, J.; Wicks, J.; Luo, M.; Wang, Z.; Agapie, T.; Peters, J. C.; Sargent, E. H.; Sinton, D. High-Rate and Efficient Ethylene Electrosynthesis Using a Catalyst/Promoter/Transport Layer. *ACS Energy Lett.* **2020**, *5* (9), 2811–2818. <https://doi.org/10.1021/acsenerylett.0c01266>.
- (34) Thevenon, A.; Rosas-Hernández, A.; Fontani Herreros, A. M.; Agapie, T.; Peters, J. C. Dramatic HER Suppression on Ag Electrodes via Molecular Films for Highly Selective CO_2 to CO Reduction. *ACS Catal.* **2021**, *11* (8), 4530–4537. <https://doi.org/10.1021/acscatal.1c00338>.

- (35) Buckley, A. K.; Cheng, T.; Oh, M. H.; Su, G. M.; Garrison, J.; Utan, S. W.; Zhu, C.; Toste, F. D.; Goddard, W. A.; Toma, F. M. Approaching 100% Selectivity at Low Potential on Ag for Electrochemical CO₂ Reduction to CO Using a Surface Additive. *ACS Catal.* **2021**, *11* (15), 9034–9042. <https://doi.org/10.1021/acscatal.1c00830>.
- (36) Kim, C.; Bui, J. C.; Luo, X.; Cooper, J. K.; Kusoglu, A.; Weber, A. Z.; Bell, A. T. Tailored Catalyst Microenvironments for CO₂ Electroreduction to Multicarbon Products on Copper Using Bilayer Ionomer Coatings. *Nat Energy* **2021**, *6* (11), 1026–1034. <https://doi.org/10.1038/s41560-021-00920-8>.
- (37) Jones, R. J. R.; Wang, Y.; Lai, Y.; Shinde, A.; Gregoire, J. M. Reactor Design and Integration with Product Detection to Accelerate Screening of Electrocatalysts for Carbon Dioxide Reduction. *Review of Scientific Instruments* **2018**, *89* (12), 124102. <https://doi.org/10.1063/1.5049704>.
- (38) Lai, Y.; Jones, R. J. R.; Wang, Y.; Zhou, L.; Gregoire, J. M. Scanning Electrochemical Flow Cell with Online Mass Spectroscopy for Accelerated Screening of Carbon Dioxide Reduction Electrocatalysts. *ACS Comb. Sci.* **2019**, *21* (10), 692–704. <https://doi.org/10.1021/acscombsci.9b00130>.
- (39) de Souza Lucas, F. W.; Zakutayev, A. Research Update: Emerging Chalcostibite Absorbers for Thin-Film Solar Cells. *APL Materials* **2018**, *6* (8), 084501. <https://doi.org/10.1063/1.5027862>.
- (40) Haddout, A.; Raidou, A.; Fahoume, M. A Review on the Numerical Modeling of CdS/CZTS-Based Solar Cells. *Appl. Phys. A* **2019**, *125* (2), 124. <https://doi.org/10.1007/s00339-019-2413-3>.
- (41) Chu, S.; Ou, P.; Ghamari, P.; Vanka, S.; Zhou, B.; Shih, I.; Song, J.; Mi, Z. Photoelectrochemical CO₂ Reduction into Syngas with the Metal/Oxide Interface. *J. Am. Chem. Soc.* **2018**, *140* (25), 7869–7877. <https://doi.org/10.1021/jacs.8b03067>.
- (42) Song, J. T.; Ryoo, H.; Cho, M.; Kim, J.; Kim, J.-G.; Chung, S.-Y.; Oh, J. Nanoporous Au Thin Films on Si Photoelectrodes for Selective and Efficient Photoelectrochemical CO₂ Reduction. *Adv. Energy Mater.* **2017**, *7* (3), 1601103. <https://doi.org/10.1002/aenm.201601103>.